European Journal of Pharmaceutics and Biopharmaceutics 78 (2011) 366–376

Contents lists available at ScienceDirect

European Journal of Pharmaceutics and Biopharmaceutics

journal homepage: www.elsevier.com/locate/ejpb

Research paper

# A new respirable form of rifampicin

Yoen-Ju Son, Jason T. McConville *

*College of Pharmacy, The University of Texas at Austin, Austin, USA*

ARTICLE INFO

*Article history:*
Received 19 August 2010
Accepted in revised form 9 February 2011
Available online 13 February 2011

*Keywords:*
Rifampicin
Polymorphism
Tuberculosis
Pulmonary
Crystal
Hydrate and dry powder inhaler

ABSTRACT

The aim of this research was to investigate a novel dry powder formulation of rifampicin (RF) that presents an improved lung deposition profile by means of a polymorphic transformation into a flake-like crystal hydrate. Rifampicin dihydrate (RFDH) was prepared by recrystallization of RF in anhydrous ethanol. A control formulation, amorphous RF (RFAM) was prepared by spray drying. The physicochemical properties of the RFDH and the RFAM were characterized. Aerosol performances of RFDH and RFAM were studied with two dry powder inhalers (DPIs), an Aerolizer® and a Handihaler®, using a Next Generation Impactor (NGI). The RFDH powder was successfully prepared using simple recrystallization process and had a MMAD of 2.2 μm. The RFDH powders were characterized as having a very thin flaky structure; this unique morphology provided improved aerosolization properties with a decreased device dependency upon aerosolization. The flaky morphology of RFDH resulted in a reduced agglomeration tendency than that of spherical RFAM particles. The maximum fine particle fraction ($FPF_{TD}$) of 68% for the RFDH was achieved with the Aerolizer® device. Significant chemical degradation was not observed from the RFDH, while the RFAM showed significant chemical degradation at 9 months. The excipient-free formulation of the RFDH offers the benefit of delivering a maximum potency formulation, of the antibiotic, directly to the site of infection, the lung.



## 1. Introduction

Tuberculosis (TB) is a chronic infectious disease, which is considered the foremost cause of death due to a single microorganism [1]. The occurrence of TB is most often due to *Mycobacterium tuberculosis* (MTB) infection, and the lung is the primary site of infection. The most common treatment for TB involves oral administration of high systemic doses of single or combined antibiotics, which causes unwanted side-effects by high systemic exposure [2]. Several current studies have been proposed for the administration of antitubercular drugs to the primary infection site, the lung, with the idea of increasing the local therapeutic effect and reduce the overall systemic exposure [3–9]. Pulmonary delivery of rifampicin (RF) has been widely studied [3–6,8,10] since it is the first choice drug in the treatment of TB [1,11]. Several respirable forms of RF, such as nano/microparticle [3–5], liposome [8], and liquid [9], have been introduced to localize the RF in the lung. However, the aerosolization properties of prepared formulations have not been adequately addressed to date and represent the most important factors in determining the drug dose to the target site. Aerosolization properties are especially important, in dry powder inhalation (DPI) formulations, as the dispersion and subsequent deposition profiles of powders are predominantly governed by the physicochemical properties of the drug and the excipient used for manufacturing [12–15].

Polymorphic transformation of drugs can be considered to be a powerful particle engineering technique in the manufacture of respirable dry powders. Improved aerosolization properties may be achieved under such transformations, since the morphology of a particle can play the most important role in powder aerodynamic performance. It has been shown that adhesion force distributions between particles can be attributed to their morphology, for instance, the surface roughness [16–18] and the crystal shape [19–21]. Several active pharmaceutical ingredients (APIs) have been successfully engineered as crystals with elongated [19,21] and flaky structures [20]. These structural changes may show significantly improved inhalation properties following polymorphic transformation [19,20,22]. Current research into respirable dry powder RF formulations are mostly focused on the amorphous form, having a spherical shape [3,4,6], due to the fact that they are prepared by a microencapsulation followed by either spray-drying or solvent evaporation processes [3,4,6]. These spherical particles may be either blended with carrier materials [6,23] or manufactured as carrier-free low-density powders containing relatively large amounts of excipient [4] to minimize adhesion forces between particles. However, low-density particles have limitations in the drug payload due to this significant quantity of incorporated excipient, and the substantial amount of RF (milligram dose) that need to be delivered to the lung for efficacy [4,5]. Additionally, the amorphous

* Corresponding author. College of Pharmacy, The University of Texas at Austin, 1 University Station, A1920, Pharmaceutics Division – PHR 4.214E, Austin, TX 78712-0126, USA. Tel.: +1 512 471 0942; fax: +1 512 471 7474.
*E-mail address:* jtmcconville@mail.utexas.edu (J.T. McConville).

0939-6411/$ - see front matter © 2011 Elsevier B.V. All rights reserved.
doi:10.1016/j.ejpb.2011.02.004

form of some investigated RF formulations may not provide long-term stability, since amorphous materials often undergo chemical degradation or recrystallization processes.

The aim of this study was to develop a novel carrier-free dry powder inhalation (DPI) formulation of RF that has improved aerodynamic properties as well as a good stability profile. It was the goal of this research to demonstrate that the use of a polymorphic transformation directly from RF crystals can offset some of the aforementioned limitations with other investigated formulation types. This study describes how the dihydrated form of RF (RFDH) was prepared from the pure RF form I, and how the crystalline structure and the physicochemical properties of RFDH were characterized by various analyses. The aerodynamic behaviors of prepared RFDH are also described with two dry powder inhalers (DPIs), the Aerolizer® and Handihaler®.

## 2. Materials and methods

### 2.1. Materials

Rifampicin (RF) was purchased from the Sigma Chemical Co. (St. Louis, MO). Size 3 hydroxypropylmethyl cellulose (HPMC) capsules were donated from Capsugel (Peapack, NJ). Polycarbonate membranes of 0.05 μm were purchased from Whatman (Florham Park, NJ). An Aerolizer® dry powder inhaler device was donated by Schering-Plough (Kenilworth, NJ). A Handihaler® device was donated from Boehringer Ingelheim GmbH (Rhein, Germany). A dissolution membrane holder was provided by Copley Scientific (Nottingham, UK). All other reagents were purchased from the Sigma Chemical Co. (St. Louis, MO).

### 2.2. Preparation of rifampicin hydrate and amorphous RF

Rifampicin dihydrate was prepared by heating the anhydrous ethanol suspension of the form I rifampicin (RF) at 60 °C. RF powder (900 mg) was added to the hot anhydrous ethanol (60 °C) solution (30 mL) and stirred until a saturated solution was obtained at room temperature. The suspension was homogenized with a Ultra-Turrax high-shear homogenizer (IKA® Works Inc., Wilmington, NC) at 10,000 rpm for 2 min to homogeneously disperse the particles. The resultant suspension was then spray-dried with constant stirring using a Büchi Minispray dryer B-290 equipped with a high-performance cyclone (Büchi Laboratory-Techniques, Flawil, Switzerland) with a 0.7-mm two-fluid nozzle. The following conditions were used during spray-drying: inlet temperature, 70 °C; spray flow rate, 500 L/h; pump setting, 15% (5 mL/min); aspirator setting, 100% (40 $m^3$/h). These conditions resulted in an outlet temperature of 40–43 °C. To measure the dissolved amount of RF in the suspension, the suspension containing recrystallized particles was prepared as described earlier and centrifuged at 10,000 rpm for 5 min, and the RF content in the supernatant was analyzed using a validated HPLC method [3].

Amorphous RF (RFAM) was prepared as a control formulation by spray-drying. One gram of RF was dissolved in 50 mL of dichloromethane and spray-dried under the same spray conditions as described earlier. The resultant powders, RFDH and RFAM were stored at ambient condition (25 °C/50% RH).

The RF content of the RF form I, RFDH, and RFAM powders were determined using HPLC. A stock solution of each sample was prepared; each powder (25 mg) was weighed separately and dissolved with 25 mL of methanol. One milliliter of each stock solution was diluted with 9 mL of mobile phase. For identification of RFDH and RFAM, a concentration of 100 μg/mL RF, RFAM, and RFDH solution were each prepared from their respective stock solutions. The prepared RF solution (10 mL) was then spiked with the RFDH and the RFAM solutions (10 mL) and analyzed using HPLC [3].

### 2.3. Characterization

#### 2.3.1. X-ray diffraction of powders

The crystalline structures of prepared samples were examined using wide angle X-ray diffraction (XRD). A Philips 1710 X-ray diffractometer (Philips Electronic Instruments Inc., Mahwah, NJ) with a copper target (Cu Kα1, $\lambda$ = 1.54056 Å) and a nickel filter, at a voltage of 40 kV and a current at 40 mA, was used to obtain the XRD patterns. Samples were analyzed in the 2-theta ($2\theta$) range from 5° to 50° using a step size of 0.02 $2\theta$° with a dwell time of 2 s.

#### 2.3.2. Thermal analysis

Thermograms were measured using a differential scanning calorimetry (DSC), Model 2920 (TA Instruments, New Castle, DE). Dry nitrogen gas was used as the purge gas through the DSC cell at a flow rate of 40 mL/min. Samples (5 mg) were weighed into aluminum crimped pans. The mass of the empty sample pan was matched with that of the empty reference pan within ±0.2 mg. Samples were heated at a ramp rate of 10 °C/min from 30 to 350 °C. Thermogravimetric analysis (TGA) was conducted using a Perkin Elmer TGA 1 system (Perkin Elmer Inc., Waltham, MA). Mass loss from 5-mg samples at a heating rate of 10 °C/min from 30 to 350 °C under nitrogen purge (40 mL/min) was recorded.

#### 2.3.3. Moisture sorption analysis

Dynamic vapor sorption (DVS) was used to investigate the moisture sorption of RFDH, RF and RFAM powders. Samples (10 mg) were pre-weighed and added to quartz sample pans that were placed in the sample chamber of a DVS-1 apparatus (Surface Measurement Systems Ltd., London, UK). During this measurement, all samples, RF, RFAM, or RFDH, were separately exposed to a continuous flow of $N_2$. Each sample was dried at 0% RH for 2 h before being exposed to 10% RH increments for two 0–90% RH cycles at 25 °C. To prevent desolvation, another condition was applied for RFDH. The humidity increments started from 50% to 90% RH. Equilibrium moisture content at each increment was determined by a dm/dt of 0.002%/min.

#### 2.3.4. Particle size distribution, density, and aerodynamic diameter

Particle size distributions, based on volume fractions of prepared powders, was measured using a Spraytec® particle size analyzer equipped with an inhalation cell (Malvern Instruments, Ltd., Worcestershire, UK). It consists of a Spraytec® unit with a USP throat held in place by the inhalation cell, and a connection for an aerosol generating device. The entire assembly was operated in a closed system and allowed for a controlled airflow rate (60 L/min) through the measurement zone. Size 3 HPMC capsules were filled with 15 mg of powder and loaded into the Aerolizer® device. The Aerolizer® device was then fired into the Spraytec® particle size analyzer at an air flow rate of 60 L/min to allow the particle size distribution of DPIs to be measured under simulated actuation conditions.

The bulk densities of the RFAM and RFDH powders were determined by pouring a known mass of powder (approximately 0.5 g) under gravity into a calibrated measuring cylinder, then recording the volume occupied by the powder. The tapped density was measured by following a USP method [24]. Theoretical estimates of aerodynamic diameter ($d_{ae}$) were derived from the particle sizing ($d_{0.5}$) and tapped density data ($p$), according to the following equation [25]:

$$d_{ae} = d \times \sqrt{\frac{\rho}{\rho_1}}, \quad \text{where} \quad \rho_1 = 1\ \text{g cm}^{-3} \tag{1}$$

*2.3.5. Scanning electron microscopy (SEM)*

The morphology of prepared samples, RF, RFAM and RFDH, was observed using a LEO 1530 SEM (Zeiss/LEO, Oberkochen, Germany). Each sample was mounted separately onto SEM stubs using double-sided copper tape before sputter coating with silver for 30 s under vacuum at 30 mTorr. The SEM was operated at high vacuum with accelerating voltage 5 kV and specimen working distance 4 mm.

*2.3.6. Hot-stage microscopy*

Thermal events of prepared samples, RFDH, RFAM, and RF, were observed on a hot stage (Mettler FP 82 HT, Mettler Instrument Corp., Highstwon, NJ) under optical microscope equipped with cross polarizer (Olympus BX 60, Olympus America Inc., Center Valley, PA). The samples were mounted on the slide glass, without a cover glass, and heated from 25 °C to 200 °C at a rate of 10 °C/min. Images were transferred via a Spot Insight QE Color 4.2 (Diagnostic Instruments, Sterling Heights, MI) and analyzed using SPOT™ imaging software (version 3.5.5).

*2.3.7. Saturation solubility*

The solubility of prepared samples, RFDH, RFAM, and RF, was determined in pH 7.4 phosphate-buffered saline (PBS) containing 0.02% (w/v) ascorbic acid as an antioxidant, to prevent the oxidative degradation of dissolved samples [3]. Samples (50 mg) were added to 20 mL of the prepared PBS and shaken for 24 h at 37 °C. Samples (1 mL) were taken from each vial at 1-, 2-, 4-, 6-, 8-, and 24-h intervals and filtered with a 0.45-μm polytetrafluoroethylene (PTFE) syringe filter. Ethanol (100 μL) was added to the 900 μL of collected samples and analyzed using a validated HPLC method [3]. The resultant equilibrium sample concentration was used to calculate the saturated solubility concentration.

*2.3.8. High-performance liquid chromatography (HPLC)*

Drug content, solubility, and dissolution samples were analyzed using a HPLC system (Waters Co., Milford, MA) with UV detection. The system consisted of a 717 plus auto sampler, 2487 dual wavelength detector, 1525 binary pump, and 1500 column heater. Chromatography was performed using a Bondapak $C_{18}$ 10 μm 3.9 × 300 mm column (Waters, Milford, MA) and a SecurityGuard™ guard column (Phenomenex®, Torrance, CA). The mobile phase, consisting of methanol, acetonitrile, and phosphate buffer solution pH 5.2 in a ratio of 50:17:33, respectively, was eluted at a flow rate of 1.2 mL/min and the UV detector was set to a wavelength 337 nm. The column temperature was maintained at 25 °C, and the volume of each sample injected was 50 μL [3].

*2.4. Aerosol classification*

The aerosolization performances of RFDH and RFAM were studied using a Next Generation Impactor (NGI) (MSP Co., Shoreview, MN). The prepared RFDH powders (7, 15, or 30 mg) and 15 mg of RFAM powders were filled into the size 3 HPMC capsules and placed into either an Aerolizer® or Handihaler® dry powder inhaler (DPI). Each capsule was pierced and actuated into the NGI though a stainless steel USP throat adapter at a flow rate of 60 L/min for 4 s. The powder deposited in the throat, in each dose collection-plate of the NGI, and in the remaining capsule, were each reconstituted with 10 mL of acetone. The powders remaining in the device were washed with 10 mL of ethanol. Collected samples were analyzed by an 8453 UV/VIS spectrophotometer (Agilent, Santa Clara, CA) at 474 nm [26].

The emitted dose (ED), defined as the percent of total loaded powder mass exiting the capsule, was determined by subtracting the amount remaining in the capsule from the initial mass loaded into the capsule. The fine particle fraction (FPF), defined as the total dose of particles with aerodynamic diameters smaller than 5 μm, was calculated via interpolation from the cumulative mass against the cutoff diameter of the respective stages of the NGI. The $FPF_{TD}$ is expressed as a percentage of the total drug dose and not of the emitted dose. Each measurement was repeated three times. The MMAD was determined by the percentage cumulative undersize on probability scale versus logarithmic aerodynamic diameter data.

*2.5. Dissolution studies*

Dissolution behaviors of air-classified RFDH and RFAM were studied by a membrane holder method previously developed by this group [27,28]. To briefly summarize, approximately 1 mg of powders from each formulation were loaded onto the membrane holder inserted in the NGI dose-plate stage 3 by aerodynamic separation using the NGI. To achieve equal powder loading into the holder, the prepared powders of RFDH (7 mg) and RFAM (10 mg) were filled into size 3 HPMC capsules, placed into the Aerolizer® device, and actuated into the NGI equipped with a gravimetric sampling cup (MSP Co. Shoreview, MN) equipped with a dissolution impaction plate (Copley Scientific, Nottingham, UK) at a flow rate of 60 L/min for 4 s. The dissolution impaction plate containing air-classified particles was removed from the gravimetric sampling cup, and a pre-soaked polycarbonate membrane was placed onto the top and sealed in place with a push-fitted sealing ring. The membrane-covered dissolution impaction plate was placed into each dissolution vessel containing 300 mL of PBS containing 0.02% of ascorbic acid. Dissolution testing was conducted at 75 rpm. The dissolution media (3 mL) was withdrawn manually using a glass syringe and filtered using a 0.45-μm PTFE syringe filter at timed intervals of 15, 30, 60, 120, 180, 240, 360, and 480 min. Fresh dissolution media (3 mL) was replaced into each vessel after sampling to maintain a constant volume. Ethanol (100 μL) was added to the 900 μL of collected samples and analyzed using the validated HPLC method, described earlier [3].

*2.6. Stability*

The prepared samples, RFAM and RFDH, were stored at ambient conditions in capped amber vials (25 °C/50% RH). Drug contents and thermal behavior using differential scanning calorimetry (DSC) of stored samples were monitored every 2 months using the method described earlier.

The desolvation behavior of RFDH was studied. The prepared powder stored in the uncapped amber vial was vacuum-dried (25 °C/5% RH) in the desiccators for 1 week. The dried samples were analyzed using DSC to confirm the desolvation, and the crystalline structure was examined using the XRD procedure described earlier.

*2.7. Statistical analysis*

Data were expressed as the mean ± standard deviation (SD). Statistical differences were studied by analysis of variance (one-way ANOVA) using Jump 7.0 software (SAS Institute Inc., Cary, NC). *P* values of less than 0.05 were considered as statistically significant.

## 3. Results

*3.1. Physicochemical characteristics*

Bulky RFDH powders were prepared as shown in Fig. 1. Flake-like RFDH crystals were the result of a polymorphic transformation

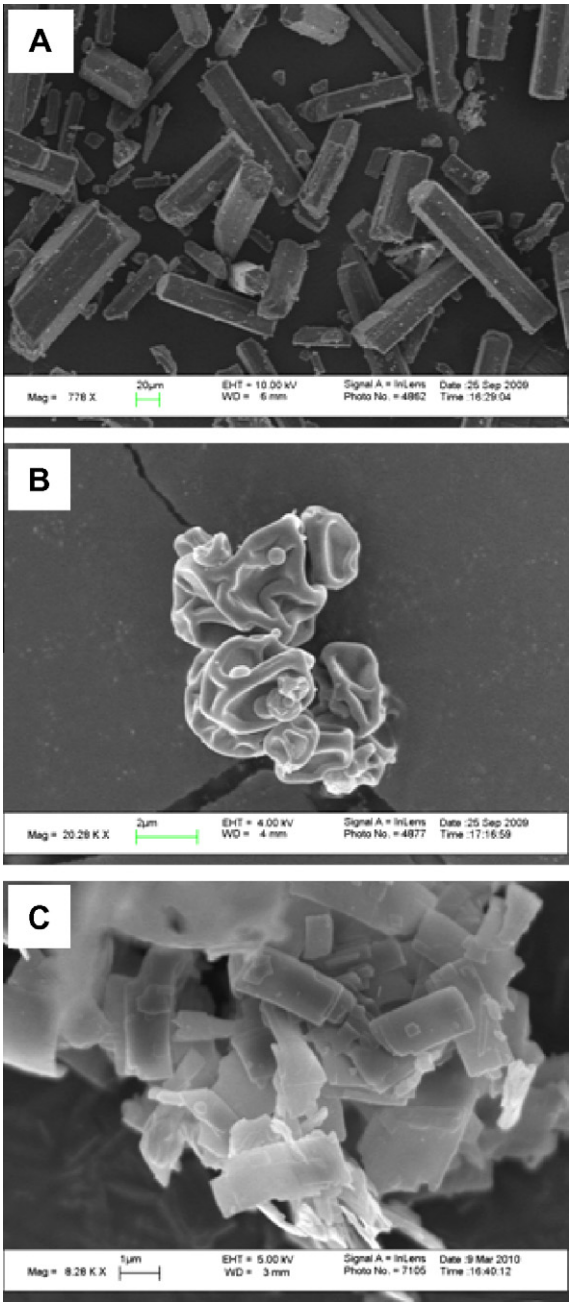


**Fig. 1.** Scanning electron microscopy images of: (A) RF form I, (B) RFAM, and (C) RFDH. (For interpretation of the references to color in this figure legend, the reader is referred to the web version of this article.)

of RF, as shown in SEM images (Fig. 1). The original crystals of RF and RFAM powders indicate a rod shape and a corrugated spherical shape, respectively (Fig. 1). The spray-dried RFDH crystals contain approximately 3.5% (w/w) of the amorphous RF form, as the dissolved RF in the suspension was also sprayed with the solid crystal.

The chemical identification for the RFDH and the RFAM samples were conducted via the spiking test. The retention time (Rt) for both spiked samples with RF was found at 5.57 min, and one completely overlapped peak was observed from the HPLC chromatogram. The RF contents of samples, RF, RFDH and RFAM, were 99.4%, 95.8% and 102%, respectively, as shown in Table 1.

The saturated solubilities of RF, RFAM, and RFDH in PBS buffer (pH 7.4) containing 0.02% (w/v) of ascorbic acid were determined to be 0.59, 1.32, and 1.28 mg/mL, respectively (Table 1). It was found that the RFDH hosts 2 mol of water per one mole of RF

**Table 1**
Physical characterizations of prepared samples, RF, RFDH, and RFAM (values are means ± SD, $n = 3$).

| | RF | RFDH | RFAM |
|---|---|---|---|
| RF contents (%) | 99.4 ± 0.47 | 95.8 ± 0.02 | 102.0 ± 1.06 |
| Yield* (%) | – | 91 ± 2.3 | 36 ± 6.3 |
| Water contents** (%) | 0.02 | 5.20 | 0.94 |
| Desolvation (°C) | – | 90–150 | – |
| Melting (°C) | – | 180 | 165 ($T_g$) |
| Decomposition (°C) | 260 | 257 | 257 |
| Solubility at 37 °C (mg/mL) | 0.59 ± 0.05 | 1.28 ± 0.01 | 1.32 ± 0.02 |

* Yield was calculated for three different batches.
** Water contents were measured by weight loss on TGA analysis.

molecule as indicated by thermal analysis. The main thermal events were summarized in Table 1. The DSC thermogram of RFDH shows two endothermic processes associated with weight loss as seen in Fig. 2A. The first one corresponds to the evaporation of physically absorbed water and the second one, at 90–150 °C, to release the water of crystallization. The dehydrated RFDH melts at 180 °C, followed by the decomposition of the product at 257 °C. From the TGA analysis (Fig. 2B), the total weight loss of 5.2% (w/w) upon drying was determined, and the weight loss corresponding to the dehydration of the water of crystallization was 4.2% (w/w). The series of thermal events for RFDH was further confirmed by hot-stage microscope (HSM) study. The transparency and brightness of crystals gradually decreased until they were melted at 180 °C while maintaining their original shape (images are not shown), indicating that desolvation causes the crystalline lattice to collapse. The thermograms of RFAM and RF were also studied (Fig. 2). In DSC and TGA analysis, no thermal event or weight loss was observed for pure RF until it decomposed at 260 °C. For the RFAM, the glass transition temperature ($T_g$) was observed at 165 °C, followed by thermal decomposition at 257 °C.

The crystalline structure of prepared samples was analyzed using XRD. As shown in Fig. 3, the characteristic peaks of the RF form I appeared at 13.65 and 14.35 2$\theta$°, respectively. The RFAM was judged to

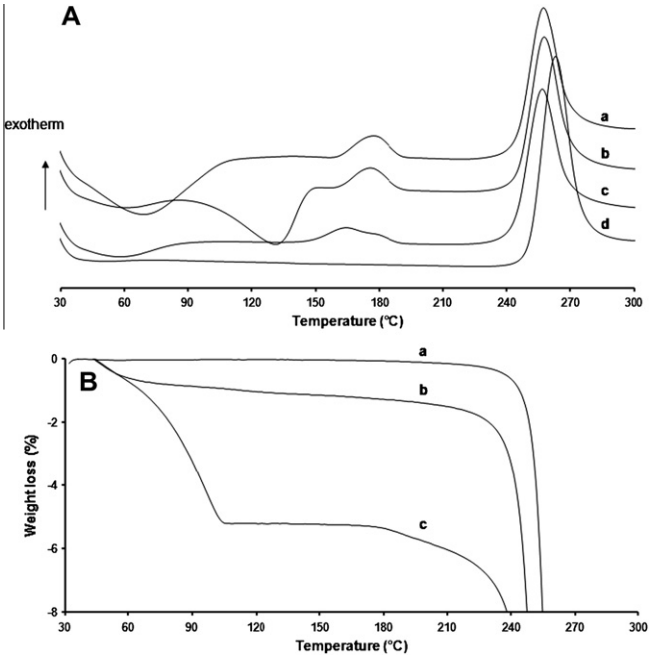


**Fig. 2.** DSC thermograms (A) of (a) desolvated RFDH (vacuum-dried for 7 days at 5% RH), (b) RFDH, (c) RFAM, and (d) RF form I, and TGA results (B) for (a) RF form I, (b) RFAM, and (c) RFDH.

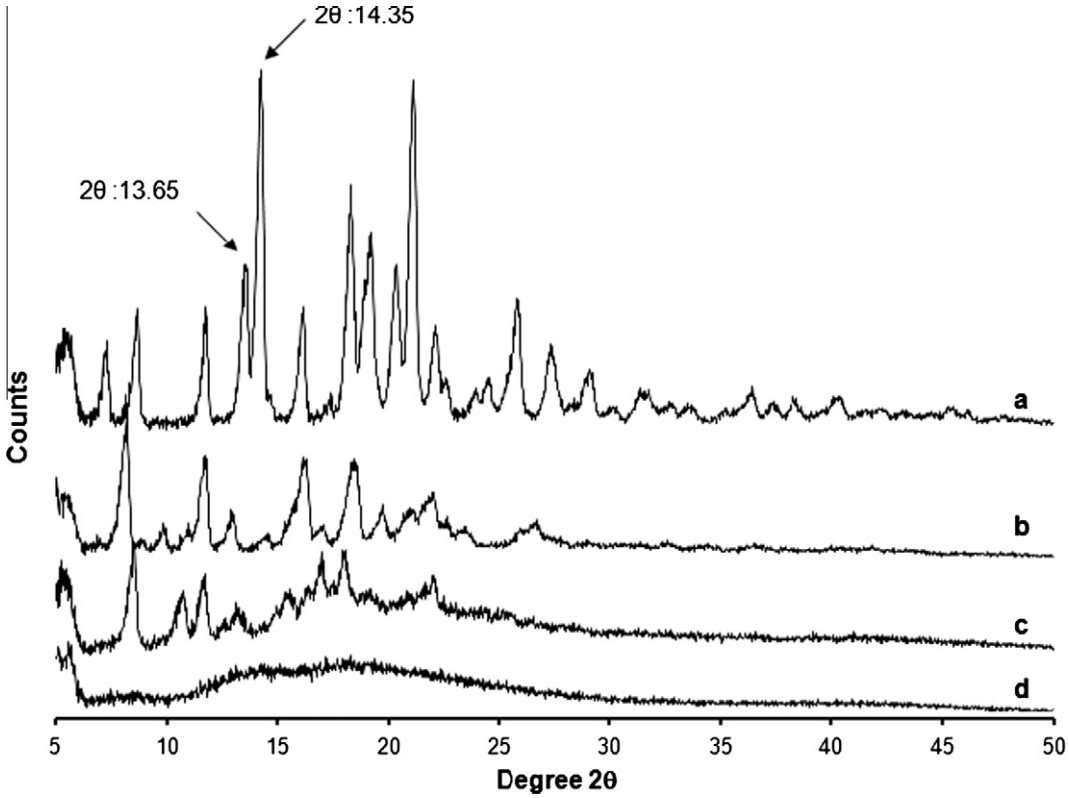


**Fig. 3.** Powder X-ray diffractograms of (a) RF form I (characterization peaks of form I: 13.65 and 14.35), (b) RFDH, (c) desolvated RFDH (vacuum-dried for 7 days at 5% RH), and (d) RFAM.

be an amorphous structure since no characteristic peaks for RF were observed, and a halo at the baseline appeared on the X-ray diffractogram. The RFDH crystal shows characteristic peaks, although the intensity of those peaks, and the subsequent degree of crystallinity, appears to be lower than that of the pure RF form. It was also found that the RFDH is a different polymorphic form than that of pure RF, as the XRD diffraction patterns were not identical. After desolvation of water from the RFDH crystal, the XRD pattern shifted, with a small halo at the baseline, indicating that the crystal lattice collapses upon desolvation as confirmed by HSM study.

Representative moisture sorption isotherms for the RFAM and the RFDH spray-dried are shown in Fig. 4A and B, respectively. In general, the two samples have very different gravimetric responses to moisture sorption. The RFAM shows large moisture uptake indicative of bulk absorption (Fig. 4A); 14% moisture uptake between 0% and 90% RH. Additionally, a remarkable and constant hysteresis between moisture sorption and desorption curves is seen on Fig. 4A, which reflects a slower diffusion of water back out of the RFAM's internal structure. Contrary to RFAM, the RFDH showed an approximately 2.3% moisture uptake between 50% and 90% RH. No remarkable hysteresis was shown from the isotherm graph (Fig. 4B). The moisture sorption study for the RFDH was conducted under two separate conditions, 0–90% RH cycle and 50–90% RH cycle; however, the 50–90% RH condition was chosen, as the RFDH showed very fast desolvation at 0% RH. The RF showed a 1% moisture uptake between 0% and 90% RH without hysteresis (graph is not shown).

The median particle sizes ($d_{0.5}$) of SP, RFAM, and RFDH were 116, 24.6, and 8.8 μm, respectively, as listed in Table 2. The RFAM and the RF powder samples showed much higher variability in particle size than that of the RFDH. It was clearly seen from Fig. 5 that the RFAM powder samples showed bimodal distribution, indicating that particles were not completely deagglomerated at the

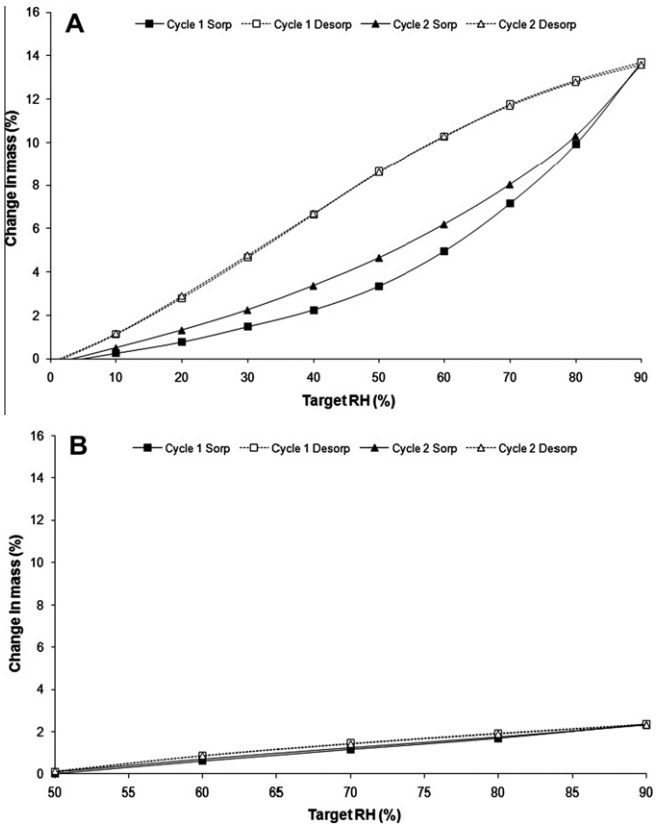


**Fig. 4.** Dynamic vapor sorption (DVS) isotherm of (A) RFAM and (B) RFDH. The absorptions are shown as solid lines and desorptions as dashed lines.

**Table 2**
Particle size characteristics of the formulations, measured with a Spraytec® light diffraction apparatus at a flow rate of 60 L/min (values are means ± SD, $n = 3$).

| Samples | $d_{0.1}$ (μm) | $d_{0.5}$ (μm) | $d_{0.9}$ (μm) | $d_{ae}$ (μm) |
|---|---|---|---|---|
| RF | 42.6 ± 4.0 | 116.0 ± 6.9 | 368.0 ± 57.0 | – |
| RFDH | 2.4 ± 0.0 | 8.8 ± 0.1 | 22.6 ± 0.7 | 2.3 ± 0.1 |
| RFAM | 2.7 ± 2.1 | 24.6 ± 7.8 | 143.0 ± 19.8 | – |

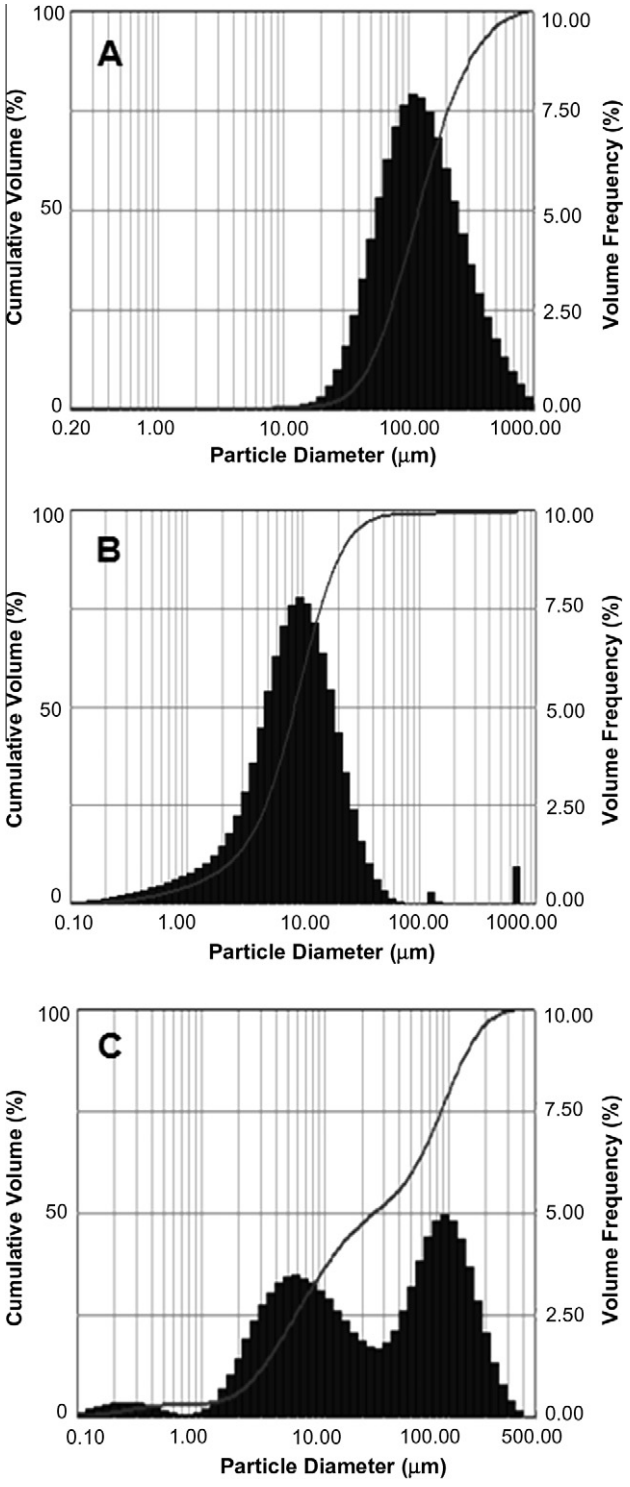


**Fig. 5.** Average particle size distribution measured by Spraytec® at a flow rate of 60 L/min for (A) RF form I, (B) RFDH, and (C) RFAM.

airflow (60 mL/min), whereas RFDH powder samples demonstrated a unimodal distribution. The calculated $d_{ae}$ value for the RFDH was 2.3 μm, and the $d_{ae}$ value for RFAM could not be obtained since the tapped density could not be measured properly due to the cohesive properties of powders.

### 3.2. Aerodynamic properties

The aerosolization properties of RFDH and RFAM were compared with two DPIs, the Aerolizer® and the Handihaler®. The ED, $FPF_{TD}$, and MMAD of RFAM and RFDH powders are displayed in Table 3. The aerodynamic performances of the RFDH powders were improved by changing the crystalline structure to a flake-like dihydrate form, with at least a $FPF_{TD}$ of 60% for each DPI device. Although the RFAM was manufactured as a highly corrugated powder to improve the dispersibility, the $FPF_{TD}$ values obtained from Handihaler® and Aerolizer® were lower than those of RFDH, at 50.9% and 36.6%, respectively. The mass of RFDH powders deposited on each dose collection-plate was not dependent on the capsule fill mass, as shown in Fig. 6. The $FPF_{TD}$ values of RFDH obtained from different capsule fill masses (7, 15, and 30 mg) were 59.1%, 63.8%, 60%, respectively, with more than 90% of the capsule contents being emitted during aerosolization testing at an air flow of 60 L/min. A difference in the mass deposition between two different devices was also found for the RFAM and the RFDH powders, as shown in Fig. 7. For RFDH, the Aerolizer® shows better particle separation than that of the Handihaler®. Conversely, for the RFAM, the Handihaler® shows better separation than the Aerolizer® as the $FPF_{TD}$ values for RFDH and RFAM were 63.8% and 50.9% with the Handihaler® device, and 68.5% and 36.6% with Aerolizer®, respectively. In particular, the ED of RFAM showed a significant difference between the two devices.

The MMAD of RFDH calculated from the Handihaler® device was in the range of 3.1–3.7 μm at an air flow of 60 L/min compared to 2.2 μm in the Aerolizer® at the same airflow. The theoretical estimate of $d_{ae}$ for RFDH powders was more similar to the MMAD value obtained from the Aerolizer® device, indicating that the Aerolizer® device is more efficient in particle deagglomeration than Handihaler®. For the RFAM, MMAD values were 2.8 and 3.4 for Aerolizer® and Handihaler®, respectively.

### 3.3. Stability

The physicochemical stabilities of the RFAM and RFDH were studied. The RF contents of stored formulations for 9 months were summarized in Table 4. No significant change in RF content was found from the RFDH samples over the 9-month study period. The DSC thermograms of RFDH for 6 months were identical to that of the initial sample, as shown in Fig. 8. Contrary to the RFDH, the RFAM showed a significant difference in drug content, which was lowered to 75.5% at 9 months. The DSC thermograms of 4 and 6 months RFAM samples show that the peaks corresponding to the $T_g$ at 165 °C are gradually shifted to 180 °C, implying the changing in the order of molecular arrangement (Fig. 8). It is also shown in the DSC thermograms in Fig. 8 that the peak corresponding to drug decomposition was broadened, and the onset of degradation was earlier than that of initial sample. A color change was also observed for the RFAM powder (image is not shown). The recrystallization of RFAM (4 month sample) was further confirmed by the HSM study. The bright interference color was observed from the 4-month samples of RFAM powder over the temperature range of 30 to 200 °C (images are not shown).

Desolvation of the water of crystallization was confirmed by the DSC study. After drying, the peak at 110–150 °C disappeared and the endothermic peak corresponding to the physically absorbed water was increased since most of the particles lost their crystalline

**Table 3**
Aerodynamic characteristics of the formulations at a flow rate of 60 L/min (values are means ± SD, $n = 3$).

| DPIs fill mass (mg) | RFDH | | | | RFAM | |
|---|---|---|---|---|---|---|
| | Handihaler® | | | Aerolizer® | Handihaler® | Aerolizer® |
| | 7 | 15 | 30 | 15 | 15 | 15 |
| ED (%) | 91.4 ± 1.5 | 97.6 ± 0.3 | 95.2 ± 1.9 | 98.3 ± 0.2 | 94.1 ± 1.7 | 56.1 ± 0.2 |
| $FPF_{TD}$ (%) | 59.1 ± 1.2 | 63.8 ± 1.5 | 60.2 ± 3.7 | 68.5 ± 2.4 | 50.9 ± 2.2 | 36.6 ± 0.4 |
| MMAD (μm) | 3.1 ± 0.2 | 3.7 ± 0.1 | 3.2 ± 0.1 | 2.2 ± 0.1 | 3.4 ± 0.3 | 2.8 ± 0.1 |

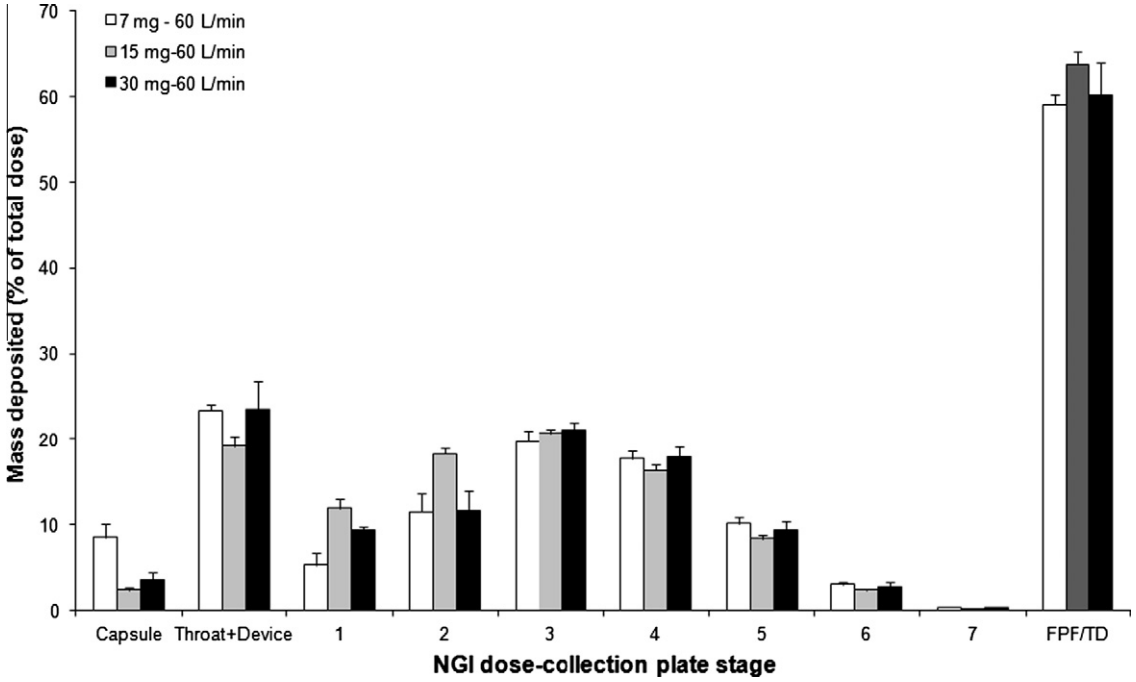


**Fig. 6.** Powder deposition profiles for RFDH having different powder fill mass at a flow rate of 60 L/min with Handihaler®, expressed as the percentage of total loaded dose (values are means ± SD, $n = 3$).

structure. Under vacuum, the desolvation was completed in 1 week. It was also found that this process was accelerated using $N_2$ gas from the DVS study.

### 3.4. Dissolution studies

Dissolution studies were performed with the RFAM and RFDH formulations. For dose collection, the particles were air-classified using NGI as explained earlier, the particles deposited on the collection-plate stage 3 were used for the dissolution study. The amount of powder deposited on stage 3 for both formulations was 1 mg. Fig. 9 shows that 74% and 82% of the RF were released for the RFDH and the RFAM samples from stage 3 within 1 h.

## 4. Discussion

### 4.1. Polymorphic transformation to the flake-like crystal of RF

The flake-like RF dihydrate crystal was prepared by recrystallization in anhydrous ethanol followed by spray-drying of the prepared suspension, as shown in Fig. 1. Generally, the drying of recrystallized particles involves heat or vacuum conditions to remove solvents used in the recrystallization process. However, those conditions may not be suitable if the prepared crystal is in the hydrate or solvate form since desolvation may occur during the drying process [29,30]. Desolvation of the hydrate form of a crystal usually results in the rearrangement of the crystal lattice, generally leading to loss of crystallinity or significant structural change [29,30]. Fig. 3 shows that the desolvation of RF causes the crystalline lattice to collapse whether it is dried via vacuum conditions or $N_2$ gas purge. The spray-drying process allows the RFDH crystals to dry without desolvation since it allows for very rapid drying. Thus, the crystals are not heated while they are drying [31]. Additionally, aggregation or caking of the RFDH particles was prevented as particles were further deaggregated by atomization involving the break-up of liquid feed into very fine droplets.

The dihydrate form of RF was confirmed by thermal analysis. The DSC thermogram of RFDH (Fig. 2A) showed an endothermic peak corresponding to the release of the water of crystallization at 90–150 °C, and the TGA weight loss for the desolvation was 4.2%, which was equivalent to 2 mol of water per mole of RF (Fig. 2B). Generally, a hydrate is formed from the aqueous media or the mixture of aqueous/organic solvent by the association of water molecules in the crystal lattice. However, in RF the formation of several hydrates, mono-, di-, and heptahydrate, from several organic solvents has been reported, which can be attributed to the traces of water in the solvents. Specifically, it was reported that the mono- and heptahydrate forms of RF are results of recrystallization from anhydrous ethanol (containing less than 1% water). These polymorphs are believed to be the product of the imbibitions of water [32,33]. The extreme complexity in the chemical structure due to the various hydrogen bonding sites and ionization states that exist may also contribute to the formation of various hydrate forms [29,30,32–34].

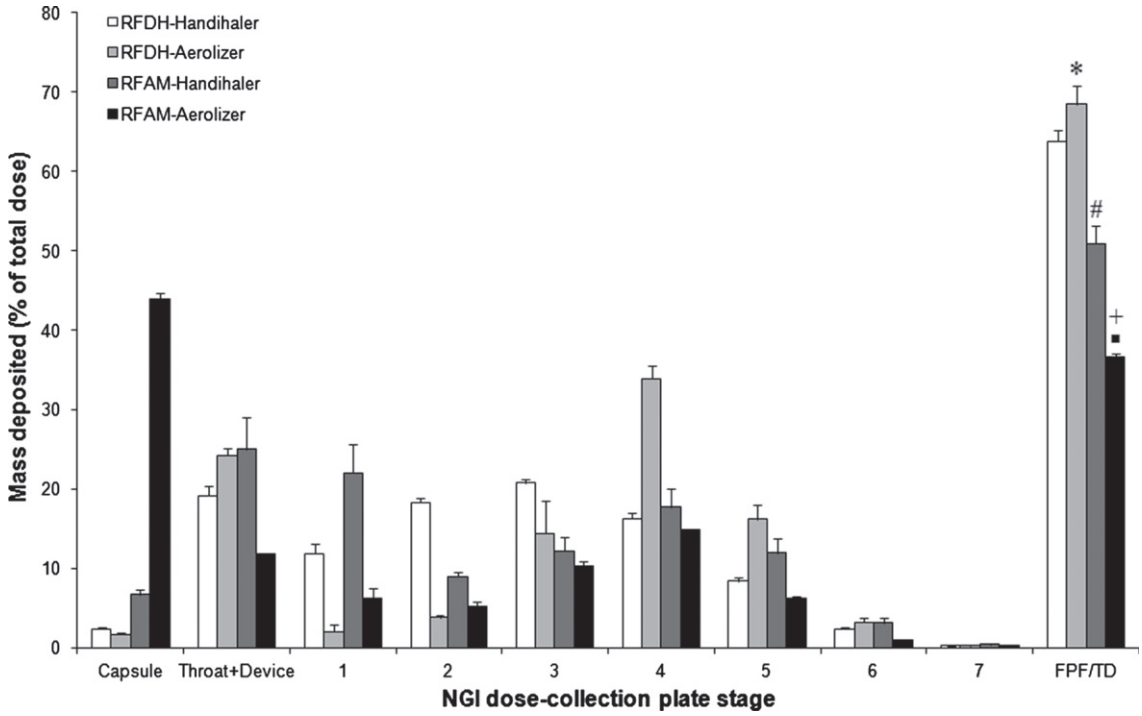


**Fig. 7.** Powder deposition profiles for the RFDH and the RFAM actuated from two different devices, Aerolizer® and Handihaler® at a flow rate of 60 L/min, expressed as the percentage of total loaded dose (values are means ± SD, $n = 3$). *The statistical difference between devices for the RFDH powders. + The statistical difference between devices for the RFAM powders. # The statistical difference between formulations for the Handihaler®. ■ The statistical difference between formulations for the Aerolizer®.

**Table 4**
RF contents analysis for the RFDH and RFAM formulations stored under ambient condition (25 °C/50% RH) over 9 months (values are means ± SD, $n = 3$).

| Samples | Initial | 2 months | 4 months | 6 months | 9 months |
|---|---|---|---|---|---|
| RFDH* | 95.8 ± 0.57 | 95.8 ± 0.02 (100%)** | 95.8 ± 0.30 (100%) | 93.8 ± 0.25 (97.9%) | 93.0 ± 0.56 (97%) |
| RFAM | 102 ± 1.06 | 91.2 ± 0.71 (89.4%) | 84.2 ± 1.06 (82.6%) | 80.8 ± 0.46 (79.2%) | 75.5 ± 0.81 (74%) |

* The drug contents of RFDH indicate RF contents.
** Values in parentheses refer to percentage decrease in RF contents.

The hydrate of RF is presumed to be a stoichiometric hydrate due to the fading of the bright interference color after dehydration on the HSM study, and to the peak shift with the halo at the baseline on the XRD diffractogram (Fig. 3), indicating that the majority of crystalline lattice was replaced to an amorphous state. This was further confirmed by DSC analysis. As indicated in Fig. 2A, the melting of dehydrated RFDH at 180 °C was not accompanied with an endothermic process since no heat was required for amorphous

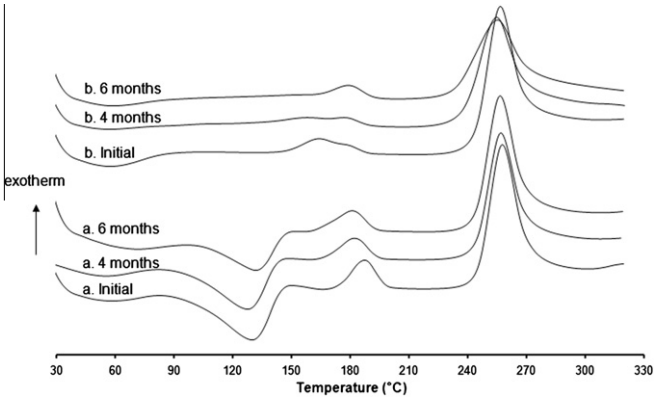


**Fig. 8.** DSC thermograms of (a) RFDH and (b) RFAM over 6 months.

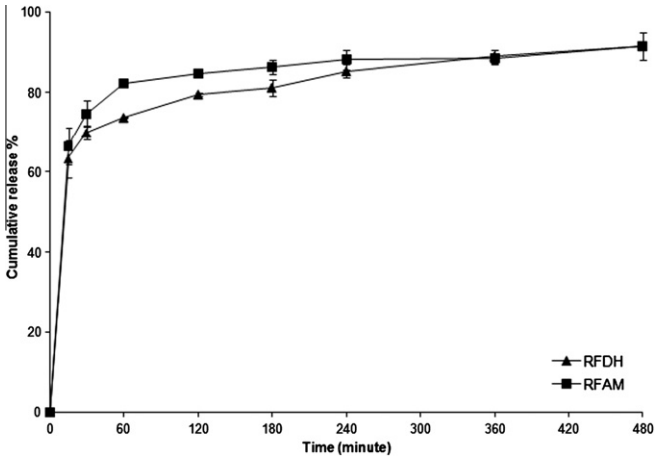


**Fig. 9.** Release profiles of RFDH and RFAM in PBS containing 0.02% ascorbic acid (pH 7.4). Powders accumulated on the dose collection-plate 3 were selected for dissolution. The error bars indicate the standard deviation of three tests.

material to pass to the liquid phase [33]. It is known that the water molecule in a stoichiometric hydrate is an essential component in the maintenance of the molecular network. Thus, desolvation of stoichiometric solvents results in a disordered crystalline state [29,30,33].

The XRD results of RFDH and RF confirm the polymorphic transformation of the RF form I to the different crystal form. Fig. 3 shows that two main characteristic peaks of the RF form I, at 13.65 and 14.35 $2\theta^{\circ}$, disappear following recrystallization, and several different characteristic peaks appear on the XRD diffractogram of RFDH although the peak intensities are relatively low. The RFDH shows less crystallinity than the RF form I, which may be attributed to the disturbed crystalline packing of the water molecule inside the crystal lattice [32,33]. The saturation solubility of RFDH was similar to that of amorphous structured RFAM, at 1.28 and 1.32 mg/mL, respectively (Table 1). This is because, although the RFDH has a crystalline structure, the packing density is low and the surface area of those two powders, RFAM and RFDH, are very large due to the small particle size.

### 4.2. Dry powder formulation and the aerodynamic properties

As seen in Fig. 1, the RFDH shows a very thin, flake-like crystal. As listed in Table 2, the median particle size ($d_{0.5}$) of the RFDH is about 8 μm, whereas the estimated aerodynamic diameter ($d_{ae}$) of 2.3 μm falls into the respirable particle size range (1–5 μm), due to the low powder density. The low-density RFDH crystals were manufactured by a very simple recrystallization process without adding any excipients, unlike other low-density dry powder formulations that generally involve complicated manufacturing processes and large amounts of excipients. The excipient-free RFDH formulation allows a high RF dose and may also prevent chemical degradation caused by drug–excipient interaction.

As shown in Fig. 7, the $FPF_{TD}$ values of RFDH powders were higher than the RFAM for both the Handihaler® and Aerolizer® devices. This is attributed to the flaky morphology and relatively large particle size ($d_{0.5}$: 8 μm) of the RFDH crystals that prevents the formation of strong aggregates with weak cohesive forces [20]. The morphology and geometric size distribution of particles has significant influence on the aerosol performance since the different particle sizes and shapes lead to a variation in surface energy and interparticulate forces [12,14,35,36]. In general, more corrugated, larger, and lower-density particles exhibit better aerosol dispersion than denser, smaller particles, due to weaker van der Waals forces, leading to easier deaggregation of particle aggregates within the air steam [12,14,16,25,37,38]. It has also been reported that powders with elongated structures provide improved aerosolization performances since the contact state between fibrous particles is extremely unstable, leading to excellent fluidization and deaggregation [19,21,22]. The unique flaky shape of RFDH powders may also contribute to the formation of unstable aggregates by reducing the particle contact area, as with elongated particles. The powder dispersion behavior of prepared formulations at a given air flow (60 L/min) was further confirmed by the particle size distribution data generated using the Spraytec® light diffraction apparatus (Fig. 5 and Table 2). As expected, it appears that the RFAM powders require more energy to be deaggregated than the RFDH, due to the strong interparticulate forces that paralleling the NGI results shown in Fig. 7. It can be clearly seen from Fig. 5 that the particle size distribution of the RFAM is very broad, with a median particle size ($d_{0.5}$) of 24.6, unlike the particle size shown in the SEM image (Fig. 1), which indicates a range of about 2–3 μm. This finding suggests that the RFAM powders form much stronger and more stable powder aggregates than the RFDH powders due to their smaller particle size and spherical shape. The significantly low yield of the RFAM powders can also be explained by the series of data mentioned earlier (Table 1). Contrary to the RFDH powder, the sprayed RFAM powders were very adhesive/cohesive. Thus, the majority of powders were lost during the spray dryer recovery process.

Significant differences in the powder dispersion behaviors were observed between two different devices for both the RFDH and RFAM formulations. The differences in $FPF_{TD}$ and ED between the two devices were more obvious for the RFAM powders than the RFDH crystals. In particular, the ED of RFAM powders obtained from the Handihaler® demonstrated an almost twofold increase when compared to the Aerlozer® device. The different particle dispersion results between two devices can be explained by the difference in the device resistance. The Aerolizer® is classified as a low-resistance device with a specific resistance of 0.056 cm $H_2O^{1/2}$/L/min [39], whereas the Handihaler® is classified as a high-resistance device with a resistance of 0.18 cm $H_2O^{1/2}$/L/min [35,40], implying the Handihaler® requires more inspiratory effort to operate the device. However, at a given flow rate, 60 L/min, a greater pressure drop across the device is achieved by the high-resistance device, the Handihaler®, than the low-resistance device, the Aerolizer®, resulting in higher shear force for powder entrainment and aerosolization. Accordingly, the higher $FPF_{TD}$ and ED for RFAM powders are attributed to the high turbulence generated within the Handihaler®, which is in general agreement with previous studies using DPI devices with different resistances; the higher the device resistance, the greater the powder deagglomeration is likely to be obtained [35,36,40].

Unexpectedly, the Aerolizer® provided maximum particle separation for the RFDH powders as the $FPF_{TD}$ values for the Aerolizer® and Handihaler® were 68.5% and 63.8%, with more than 95% of capsule contents being emitted from both devices. The differences in the particle deposition on each NGI dose-plate between two different devices were also found. As shown in Fig. 7, 5.8% and 30% of the RFDH powders were deposited at the earlier stages (stages 1 and 2) of NGI with maximum deposition at stages 4 and 3 for the Aerolizer® and Handihaler® devices, respectively. These results suggest that parts of the RFDH powders are emitted without being crushed to fine particles by the dispersion force of the airstream in the Handihaler®. This may be due to the differences in the powder emptying mechanism through the capsule apertures between two devices. The size of the apertures on the capsule end pierced by the Hadihaler® is bigger than that of the Aerolizer®, resulting in faster powder emptying from the capsule. A large aperture on the capsule allows agglomerates to readily empty from the capsule, but at the same time causes impaction at the earlier impactor stages and thus reduces the FPF [41]. Therefore, the lower $FPF_{TD}$ for the Handihaler® is attributed to the shorter powder emptying time, which is not enough time for all particle aggregates to be crushed into separated single particles. The similar MMAD (2.2 μm) and $d_{ae}$ (2.3 μm) of the RFDH further confirmed that the Aerolizer® device was more efficient in particle deagglomeration for this sample than the Handihaler® device. The emitted RFAM powders from two different devices showed similar powder distribution behavior to that of the RFDH powders. As shown in Fig. 7, emitted RFAM powders show maximum deposition at throat/device and stage 4 for the Handihaler® and for the Aerolizer®, although the $FPF_{TD}$ values were higher for the Handihaler® than for the Aerolizer® due to the higher ED from the Handihaler® device. This data indicates that larger apertures may be better for withdrawal of highly aggregated RFAM from the capsule. However, the emitted particle aggregates from the capsule having larger apertures may not be completely deaggreagated due to the short powder emptying time. Overall, the differences in ED, powder distribution, and $FPF_{TD}$ between devices for the RFDH are less significant than for the RFAM since the RFDH powders do not require much energy to be aerosolized, implying that the

device-dependent aerosolization performances can be minimized by using an engineered RFDH formulation.

The aerodynamic performances of RFDH were not dependent on the capsule fill mass since the powders were very bulky; thus, the particles were not closely packed even at higher fill mass (30 mg), as shown in Fig. 6. The $FPF_{TD}$ of RFDH obtained at different capsule fill masses (7, 15, and 30 mg) was at least 59% with more than 90% of ED at an air flow of 60 L/min. The particle deposition profiles on each dose-plate of NGI for three different samples (powder fill mass) were shown to be very similar each other.

### 4.3. Dissolution

As shown in Fig. 9, the release rate for the RFDH and the RFAM at 1 h were 74% and 82%, respectively. Overall, release patterns between the two samples in the PBS media (pH 7.4) were similar, although differences in crystalline structure exist, due to the small particle size of powders loaded on the membrane holder. The dissolution profile of RFDH was relatively slower for the first 4 h than that of the RFAM and became similar to that of the RFAM at 8 h. This result was in good agreement with the saturated solubility data; the saturation solubility between two formulations was similar, but the RFDH showed much slower powder wetting than the RFAM (saturation solubility graph is not shown). In general, amorphous structured material is believed to provide higher solubility and faster dissolution rates than crystalline materials. However, in RF, the amorphous form shows the slowest dissolution rate, although the intrinsic dissolution rate (IDR) and the saturation solubility are not significantly different from that of the crystalline RF [34,42,43]. This behavior is attributed to the electrostatic properties of the very fine particles in the amorphous powders, leading to poor powder wetting [34,42,43]. It has been reported that when the amorphous RF powders are added to the dissolution media, they forms lumps as well as a hydrophobic layer on the dissolution media surface [43]. Therefore, to obtain accurate dissolution results, particle separation should be considered prior to dissolution assessment. Specifically, the test compound is very small and cohesive like the RFAM and RFDH powders. In our previous study, we proved that the aerodynamic classification of aggregated powders has a significant influence on the dissolution profiles [27,28]. Thus, a new membrane holder method, designed specifically to be incorporated into the Next Generation Impactor (NGI) for easy particle separation, was applied to properly compare the dissolution profiles of the manufactured formulations. From the dissolution study, similar dissolution profiles between two different RF polymorphs were obtained. This result is attributed to the good separation of powders.

RF has a pH-dependent dissolution profile [3,32,34]. The RF dissolves and decomposes immediately in low pH media (pH 1.2), but slowly in neutral conditions [32,34]. This pH-dependent dissolution may indicate that the release rate of inhaled RF is potentially retarded in the lung compared to when it is delivered to the GI tract. A comparison study by Jang et al. clearly shows that RF formulations delivered to the lung showed higher plasma concentrations and a longer plasma duration than that of orally delivered RF following an *in vivo* pharmacokinetic study, although the *in vitro* dissolution profiles of prepared formulations were similar at neutral pH (pH 7.2) [4]. This could be attributed to the pH-dependent dissolution behavior of RF, as it is a class II drug of the Biopharmaceutic Classification System (BCS), where rate and extent of dissolution is critical for optimum bioavailability [34]. Additionally, it is widely known that the high variability in RF bioavailability is caused by the different solubility profiles between commercial RF forms [34,42]. Therefore, we can expect that several drawbacks in current oral delivery systems mainly involved with severe chemical decomposition and fast dissolution of RF in the acidic conditions of the stomach [44–46] can be avoided by delivering RF to the lung that has a neutral milieu.

### 4.4. Stability studies

While Table 4 shows that the chemical potency of RFDH decreases by only 3% after 9 months at ambient storage conditions, the RFAM shows significant decrease in drug content (26%). These results can be explained through the moisture uptake behavior of two formulations studied using DVS analysis. As shown in Fig. 4A, the RFAM powders take up 14% moisture between 0% and 90% RH and 10.3% moisture between 50% and 90% RH. A large hysteresis on the isotherm graph between sorption and desorption was also shown, indicating that water absorbed from the atmosphere can be diffused into the RFAM's internal structure, and the chemical degradation or the crystalline structural rearrangement could be accelerated by this. It has been reported that the primary degradation product of RF in solid state is an isonicotinyl hydrazone of 3-formylrifamycin, and the degradation is accelerated in the presence of moisture and/or light [47]. Contrary to the RFAM, the RFDH showed a 2.3% moisture uptake between 50% and 90% RH, and the hysteresis was not significant since the crystalline materials were less hygroscopic than the amorphous structure. The stabilities of the RFAM and RFDH were further confirmed by the DSC and the HSM study (Fig. 8). The bright interference color was observed for the RFAM powder at 4 months, and the bright color did not completely disappear upon heating to its $T_g$, indicating the presence of crystallized forms of RF or RF degradation product (images are not shown).

## 5. Conclusion

The rifampicin dihydrate (RFDH) powders having MMAD of 2.2 μm were successfully prepared using a simple recrystallization process. The RFDH powders have a thin flaky structure, and this unique morphology provides improved aerosolization properties at maximal API loading. The maximum $FPF_{TD}$ of the RFDH achieved with Aerolizer® device, was 68%. These powders are predicted to deposit predominately in the central and peripheral regions of the lung following inhalation, with minimal oropharyngeal deposition. RFDH powders delivered via the pulmonary route would be anticipated to provide higher local (lung) drug concentrations than that of orally delivered powders. Additionally, RFDH powders can be estimated to have much better stability than the amorphous RFAM.

## References

[1] Rifampin, Tuberculosis 88 (2) (2008) 151–154.
[2] J. Schreiber, G. Zissel, U. Greinert, M. Schlaak, J. Muller-Quernheim, Lymphocyte transformation test for the evaluation of adverse effects of antituberculous drugs, European Journal of Medicinal Chemistry 4 (2) (1999) 67–71.
[3] P. O'Hara, A.J. Hickey, Respirable PLGA microspheres containing rifampicin for the treatment of tuberculosis: manufacture and characterization, Pharmaceutical Research 17 (8) (2000) 955–961.
[4] J.C. Sung, D.J. Padilla, L. Garcia-Contreras, J.L. VerBerkmoes, D. Durbin, C.A. Peloquin, K.J. Elbert, A.J. Hickey, D.A. Edwards, Formulation and pharmacokinetics of self-assembled rifampicin nanoparticle systems for pulmonary delivery, Pharmaceutical Research 26 (8) (2009) 1847–1855.
[5] S. Suarez, P. O'Hara, M. Kazantseva, C.E. Newcomer, R. Hopfer, D.N. McMurray, A.J. Hickey, Respirable PLGA microspheres containing rifampicin for the treatment of tuberculosis: screening in an infectious disease model, Pharmaceutical Research 18 (9) (2001) 1315–1319.
[6] S. Suarez, P. O'Hara, M. Kazantseva, C.E. Newcomer, R. Hopfer, D.N. McMurray, A.J. Hickey, Airways delivery of rifampicin microparticles for the treatment of tuberculosis, Journal of Antimicrobial Chemotherapy 48 (3) (2001) 431–434.
[7] R. Sharma, D. Saxena, A.K. Dwivedi, A. Misra, Inhalable microparticles containing drug combinations to target alveolar macrophages for treatment of pulmonary tuberculosis, Pharmaceutical Research 18 (10) (2001) 1405–1410.

[8] S.P. Vyas, M.E. Kannan, S. Jain, V. Mishra, P. Singh, Design of liposomal aerosols for improved delivery of rifampicin to alveolar macrophages, International Journal of Pharmaceutics 269 (1) (2004) 37–49.
[9] F. Tewes, J. Brillault, W. Couet, J.C. Olivier, Formulation of rifampicin–cyclodextrin complexes for lung nebulization, Journal of Controlled Release 129 (2) (2008) 93–99.
[10] F. Ito, K. Makino, Preparation and properties of monodispersed rifampicin-loaded poly(lactide-co-glycolide) microspheres, Colloids and Surfaces B – Biointerfaces 39 (1–2) (2004) 17–21.
[11] C. Becker, J.B. Dressman, H.E. Junginger, S. Kopp, K.K. Midha, V.P. Shah, S. Stavchansky, D.M. Barends, Biowaiver monographs for immediate release solid oral dosage forms: rifampicin, Journal of Pharmaceutical Sciences 98 (7) (2009) 2252–2267.
[12] H.K. Chan, What is the role of particle morphology in pharmaceutical powder aerosols?, Expert Opinion on Drug Delivery 5 (8) (2008) 909–914
[13] D. Traini, P.M. Young, F. Thielmann, M. Acharya, The influence of lactose pseudopolymorphic form on salbutamol sulfate-lactose interactions in DPI formulations, Drug Development and Industrial Pharmacy 34 (9) (2008) 992–1001.
[14] H.K. Chan, Dry powder aerosol drug delivery – opportunities for colloid and surface scientists, Colloids and Surfaces A – Physicochemical and Engineering Aspects 284 (2006) 50–55.
[15] X.M. Zeng, G.P. Martin, C. Marriott, J. Pritchard, The effects of carrier size and morphology on the dispersion of salbutamol sulphate after aerosolization at different flow rates, Journal of Pharmacy and Pharmacology 52 (10) (2000) 1211–1221.
[16] S. Adi, H. Adi, P. Tang, D. Traini, H.K. Chan, P.M. Young, Micro-particle corrugation, adhesion and inhalation aerosol efficiency, European Journal of Pharmaceutical Sciences 35 (1–2) (2008) 12–18.
[17] N.Y.K. Chew, H.K. Chan, Use of solid corrugated particles to enhance powder aerosol performance, Pharmaceutical Research 18 (11) (2001) 1570–1577.
[18] N. Islam, P. Stewart, I. Larson, P. Hartley, Surface roughness contribution to the adhesion force distribution of salmeterol xinafoate on lactose carriers by atomic force microscopy, Journal of Pharmaceutical Sciences 94 (7) (2005) 1500–1511.
[19] K. Ikegami, Y. Kawashima, H. Takeuchi, H. Yamamoto, N. Isshiki, D. Momose, K. Ouchi, Improved inhalation behavior of steroid KSR-592 in vitro with Jethaler (R) by polymorphic transformation to needle-like crystals (beta-form), Pharmaceutical Research 19 (10) (2002) 1439–1445.
[20] T.T. Hu, H. Zhao, L.C. Jiang, Y. Le, J.F. Chen, J. Yun, Engineering pharmaceutical fine particles of budesonide for dry powder inhalation (DPI), Industrial & Engineering Chemistry Research 47 (23) (2008) 9623–9627.
[21] H.K. Chan, I. Gonda, Physicochemical characterization of a new respirable form of nedocromil, Journal of Pharmaceutical Sciences 84 (6) (1995) 692–696.
[22] H.K. Chan, I. Gonda, Respirable form of crystals of cromoglycic acid, Journal of Pharmaceutical Sciences 78 (2) (1989) 176–180.
[23] M.A. Darbandi, N.A. Rouholamini, K. Gilani, H. Tajerzadeh, The effect of vehicles on spray drying of rifampicin inhalable microparticles: in vitro and in vivo evaluation, Daru-Journal of Faculty of Pharmacy 16 (3) (2008) 128–135.
[24] USP32-NF27 General Chapter (616), 2009.
[25] D.A. Edwards, J. Hanes, G. Caponetti, J. Hrkach, A. BenJebria, M.L. Eskew, J. Mintzes, D. Deaver, N. Lotan, R. Langer, Large porous particles for pulmonary drug delivery, Science 276 (5320) (1997) 1868–1871.
[26] K. Tomoda, K. Makino, Effects of lung surfactants on rifampicin release rate from monodisperse rifampicin-loaded PLGA microspheres, Colloids and Surfaces B – Biointerfaces 55 (1) (2007) 115–124.
[27] Y.-J. Son, M. Horng, M. Copley, J.T. McConville, Optimization of an in vitro dissolution test method for inhalation formulations, Dissolution Technologies 17 (2) (2010) 6–13.
[28] Y.-J. Son, J.T. McConville, Development of a standardized dissolution test method for inhaled pharmaceutical formulations, International Journal of Pharmaceutics 382 (1–2) (2009) 15–22.
[29] H.G. Brittain, Polymorphism in Pharmaceutical Solids, Informa Healthcare, New York, 2009.
[30] R. Hilfiker, Polymorphism in the Pharmaceutical Industry, Wiley-VCH, Weinheim, 2006.
[31] K. Masters, Spray Drying Handbook, Longman Scientific & Technical, 1991.
[32] S.Q. Henwood, W. Liebenberg, L.R. Tiedt, A.P. Lotter, M.M. de Villiers, Characterization of the solubility dissolution properties of several new rifampicin polymorphs, solvate, and hydrates, Drug Development and Industrial Pharmacy 27 (10) (2001) 1017–1030.
[33] G. Pelizza, M. Nebuloni, P. Ferrari, G.G. Gallo, Polymorphism of rifampicin, Farmaco-Edizione Scientifica 32 (7) (1977) 471–481.
[34] S. Agrawal, Y. Ashokraj, P.V. Bharatam, O. Pillai, R. Panchagnula, Solid-state characterization of rifampicin samples and its biopharmaceutic relevance, European Journal of Pharmaceutical Sciences 22 (2–3) (2004) 127–144.
[35] M.D. Louey, M. Van Oort, A.J. Hickey, Aerosol dispersion of respirable particles in narrow size distributions produced by jet-milling and spray-drying techniques, Pharmaceutical Research 21 (7) (2004) 1200–1206.
[36] M.D. Louey, M. Van Oort, A.J. Hickey, Aerosol dispersion of respirable particles in narrow size distributions using drug-alone and lactose-blend formulations, Pharmaceutical Research 21 (7) (2004) 1207–1213.
[37] H. Adi, D. Traini, H.K. Chan, P.M. Young, The influence of drug morphology on the aerosolisation efficiency of dry powder inhaler formulations, Journal of Pharmaceutical Sciences 97 (7) (2008) 2780–2788.
[38] L.A. Dellamary, T.E. Tarara, D.J. Smith, C.H. Woelk, A. Adractas, M.L. Costello, H. Gill, J.G. Weers, Hollow porous particles in metered dose inhalers, Pharmaceutical Research 17 (2) (2000) 168–174.
[39] C.P. Criee, T. Meyer, W. Petro, K. Sommerer, P. Zeising, In vitro comparison of two delivery devices for administering formoterol: Foradil (R) P and formoterol ratiopharm single-dose capsule inhaler, Journal of Aerosol Medicine-Deposition Clearance and Effects in the Lung 19 (4) (2006) 466–472.
[40] T. Srichana, G.P. Martin, C. Marriott, Dry powder inhalers: the influence of device resistance and powder formulation on drug and lactose deposition in vitro, European Journal of Pharmaceutical Sciences 7 (1) (1998) 73–80.
[41] N.Y.K. Chew, H.K. Chan, D.F. Bagster, J. Mukhraiya, Characterization of pharmaceutical powder inhalers: estimation of energy input for powder dispersion and effect of capsule device configuration, Journal of Aerosol Science 33 (7) (2002) 999–1008.
[42] S.Q. Henwood, M.M. de Villiers, W. Liebenberg, A.P. Lotter, Solubility and dissolution properties of generic rifampicin raw materials, Drug Development and Industrial Pharmacy 26 (4) (2000) 403–408.
[43] R. Panchagnula, V. Bhardwaj, Effect of amorphous content on dissolution characteristics of rifampicin, Drug Development and Industrial Pharmacy 34 (6) (2008) 642–649.
[44] R. Sankar, N. Sharda, S. Singh, Behavior of decomposition of rifampicin in the presence of isoniazid in the pH range 1–3, Drug Development and Industrial Pharmacy 29 (7) (2003) 733–738.
[45] C.J. Shishoo, S.A. Shah, I.S. Rathod, S.S. Savale, J.S. Kotecha, P.B. Shah, Stability of rifampicin in dissolution medium in presence of isoniazid, International Journal of Pharmaceutics 190 (1) (1999) 109–123.
[46] S. Singh, T.T. Mariappan, R. Sankar, N. Sarda, B. Singh, A critical review of the probable reasons for the poor/variable bioavailability of rifampicin from anti-tubercular fixed-dose combination (FDC) products, and the likely solutions to the problem, International Journal of Pharmaceutics 228 (1–2) (2001) 5–17.
[47] H. Bhutani, T.T. Mariappan, S. Singh, The physical and chemical stability of anti-tuberculosis fixed-dose combination products under accelerated climatic conditions, International Journal of Tuberculosis and Lung Disease 8 (9) (2004) 1073–1080.